Letter | Editors' Suggestion

Transport and magnetic properties of Hund's metal $CaRuO_3$ under strain modulation

Zhen Wang,[1,2,3] Arjyama Bordoloi,[4] Zhaoqing Ding,[2,5] Enling Wang,[2,5] Xiaofeng Wu,[2,5] Zeguo Lin,[2,5] Mingyu Yang,[2,5] Chenxu Liu,[1,3] Jinglin Zhou,[1,3] Meng Meng,[2] Fang Yang,[2] Qinghua Zhang,[2] Xiaoran Liu,[2,*] Sobhit Singh,[4,6] Huan-hua Wang,[1,3,†] and Jiandong Guo[2,5,‡]

[1]*Institute of High Energy Physics, Chinese Academy of Sciences, Beijing 100049, China*

[2]*Beijing National Laboratory for Condensed Matter Physics and Institute of Physics, Chinese Academy of Sciences, Beijing 100190, China*

[3]*School of Nuclear Science and Technology, University of Chinese Academy of Sciences, Beijing 100049, China*

[4]*Department of Mechanical Engineering, University of Rochester, Rochester, New York 14627, USA*

[5]*School of Physical Sciences, University of Chinese Academy of Sciences, Beijing 100049, China*

[6]*Materials Science Program, University of Rochester, Rochester, New York 14627, USA*

(Received 13 March 2024; revised 23 May 2024; accepted 28 June 2024; published 11 July 2024)

We synthesized $CaRuO_3$ (001) thin films on a set of substrates and investigated their electronic and magnetic properties via combining magnetotransport measurements with first-principles density-functional theory calculations. The experimental results indicate that a moderate strain can introduce the Kondo effect in the system, leading to a significant modulation of the non-Fermi liquid behavior. Moreover, when the strain reaches a certain threshold, the system undergoes a metal-semiconductor transition, accompanied by a transition from a nonmagnetic state to a plausible G-type antiferromagnetic state. We attribute the observed phenomena in $CaRuO_3$ to strain-induced disruption of the delicate balance between the itinerant and the local Ru 4*d* electrons. These findings shed light on the intriguing magnetic and non-Fermi liquid behavior of $CaRuO_3$, systematically tailored by heteroepitaxial strain.

DOI: 10.1103/PhysRevB.110.L041403

Introduction. A diverse array of strongly correlated physical phenomena emerged in complex oxides with intricate coupling of multiple degrees of freedom, such as metal-insulator transitions, high-temperature superconductivity, heavy fermion effects, colossal magnetoresistance, and charge density waves [1–8]. The non-Fermi liquid (NFL) behavior—a collective term for quantum liquids that defy the Landau Fermi-liquid (FL) paradigm—is prevalent in these strongly correlated systems [9]. In NFLs the electron-electron interactions are significantly pronounced, leading to exotic electronic properties, such as power-law behavior in resistivity, anomalous specific heat, unconventional magnetic responses, etc. [9,10].

As representative NFLs, the perovskite ruthenates $ARuO_3$ (A = Ca or Sr) have attracted tremendous interest in recent years [11–17]. They assume the $GdFeO_3$-type orthorhombic structure with the *Pbnm* symmetry, and the RuO_6 octahedra are tilted by approximately 10° in $SrRuO_3$ and 17° in $CaRuO_3$ away from the ideal cubic structure [15]. Due to stronger hybridization between O 2*p* and Ru 4*d* orbitals, the t_{2g}-e_g splitting is larger compared to the 3*d* counterparts, resulting in a low-spin (LS) $S = 1$ configuration [14,15]. $SrRuO_3$ has drawn widespread attention owing to the itinerant ferromagnetism with a Curie temperature $T_C = 160$ K and the rich topological properties [12,18,19]. Its FL transition temperature T_{FL} is around 15 K, above which the disappearance of quantum oscillations and the absence of the T^2 dependence of resistance indicate the emergence of NFL behavior [10,20,21]. In the regime where $T_C > T > T_{FL}$, the temperature dependence of the resistance exhibits a power law behavior with an exponent of 1.5; In the $T > T_C$ regime, the exponent changes to 0.5 [20,21].

As the sister compound, $CaRuO_3$ displays distinct features driven by stronger RuO_6 octahedral tilting [17,22]. While there is currently considerable controversy regarding the understanding of $CaRuO_3$, some foundational experimental facts have been established. As temperature decreases, $CaRuO_3$ does not establish long-range ferromagnetic order like $SrRuO_3$, and its T_{FL} is much lower at only ~1.5 K [23]. Within 2–15 K, the resistance exhibits the power-law behavior with the exponent of 1.5, and upon further increasing temperature, it crosses over to the 0.5 exponent in the range from 40 K to 300 K [24]. Strikingly, despite the absence of ferromagnetism and differences in the overall temperature scales, the power-law behaviors of $CaRuO_3$ in all three temperature regimes closely resemble those of $SrRuO_3$. This would suggest a common origin for the strongly correlated behavior in both materials. Many theoretical investigations have concentrated on this aspect [17,25], and one notable avenue of exploration is the Hund's metal mechanism [10,14,23]. Furthermore, the similarity in electrical transport properties also raises the question about the appropriateness of treating $CaRuO_3$'s ground state as a trivial paramagnet, remaining as a topic of debate with no consensus to date [13,26–30].

*Contact author: xiaoran.liu@iphy.ac.cn
†Contact author: wanghh@ihep.ac.cn
‡Contact author: jdguo@iphy.ac.cn

Earlier prevailing viewpoints suggested that the ground state of $CaRuO_3$ is located near a ferromagnetic quantum critical point [17,22,31], supported by the *ab initio* calculations revealing the possibility of transition from a nonmagnetic state to a ferromagnetic state by doping or under certain tensile strain [32,33]. However, this prediction has yet to be experimentally verified in pure-phase $CaRuO_3$.

In this work, we synthesized (001)-oriented (in pseudocubic notation) $CaRuO_3$ thin films on different substrates and investigated their electronic and magnetic properties via magnetotransport measurements and first-principles density-functional theory calculations. The experimental results indicate that even a small amount of biaxial in-plane tensile strain can introduce the Kondo effect in $CaRuO_3$, leading to a significant modulation of magnetoresistance (MR). With increasing tensile strain, the Kondo effect becomes more pronounced, and the power-law relationship representing the NFL behavior of $CaRuO_3$ is noticeably modulated. Essentially, when the strain reaches a certain threshold, the system undergoes a metal-insulator transition, likely accompanied by an antiferromagnetic phase transition, which is consistent with the results of our theoretical calculations. We attribute these behaviors to the strain-induced disruption of the delicate balance between itinerancy and localization of the Ru $4d$ electrons.

Methods. $CaRuO_3$ epitaxial thin films were fabricated using the pulsed laser deposition (PLD) technique at a substrate temperature of ∼775 °C and under the oxygen pressure of ∼1 Pa. Five different substrates, i.e., $NdGaO_3$ (NGO), $(La, Sr)(Al, Ta)O_3$ (LSAT), $SrTiO_3$ (STO), $TbScO_3$ (TSO), and $GdScO_3$ (GSO) were used, covering the strain range from 0.44% to 3.20%. The structural characterizations of the $CaRuO_3$ films in reciprocal space were performed at beamline 1W1A of the Beijing Synchrotron Radiation Facility (BSRF), utilizing x-ray diffraction (XRD), x-ray reflectivity (XRR), rocking curves (RC), and reciprocal space mapping (RSM) to systematically investigate the film's phase, thickness, crystallinity, and in-plane strain status. The magnetotransport experiments were carried out using the van der Pauw method on a physical property measurement system (PPMS, Quantum Design). During the measurements, the magnetic field was applied perpendicular to the sample surface. To extract the pure MR signals, the symmetrization treatments were employed on the raw data.

First-principles density-functional theory (DFT + U) calculations [34,35] were performed using the projector augmented-wave (PAW) method [36] as implemented in the Vienna *ab initio* simulation package (VASP) [37–39]. The effect of in-plane biaxial strain was systematically investigated by varying the a and b lattice parameters, while freely relaxing the c lattice parameter. The Brillouin zone was sampled using a Monkhorst-Pack [40] k mesh of size 12 × 12 × 9, and the kinetic energy cutoff for the plane wave basis set was set to 600 eV. The exchange-correlation part of the Hamiltonian was computed using the generalized-gradient approximation as parametrized by Perdew, Burke, and Ernzerhof for solids (PBEsol) [41]. In the PAW pseudopotential, we considered contributions from ten valence electrons ($3s^2 3p^6 4s^2$) for Ca, eight valence electrons ($4d^7 5s^1$) for Ru, and six valence electrons ($2s^2 2p^4$) for O. All the inneratomic coordinates were fully optimized for each strain configuration until the residual Hellmann-Feynman forces were less than 10^{-3} eV/Å per atom. The energy convergence criteria for the electronic self-consistent calculations were set to 10^{-7} eV. The VASPKIT package was utilized for postprocessing the electronic structure data [42].

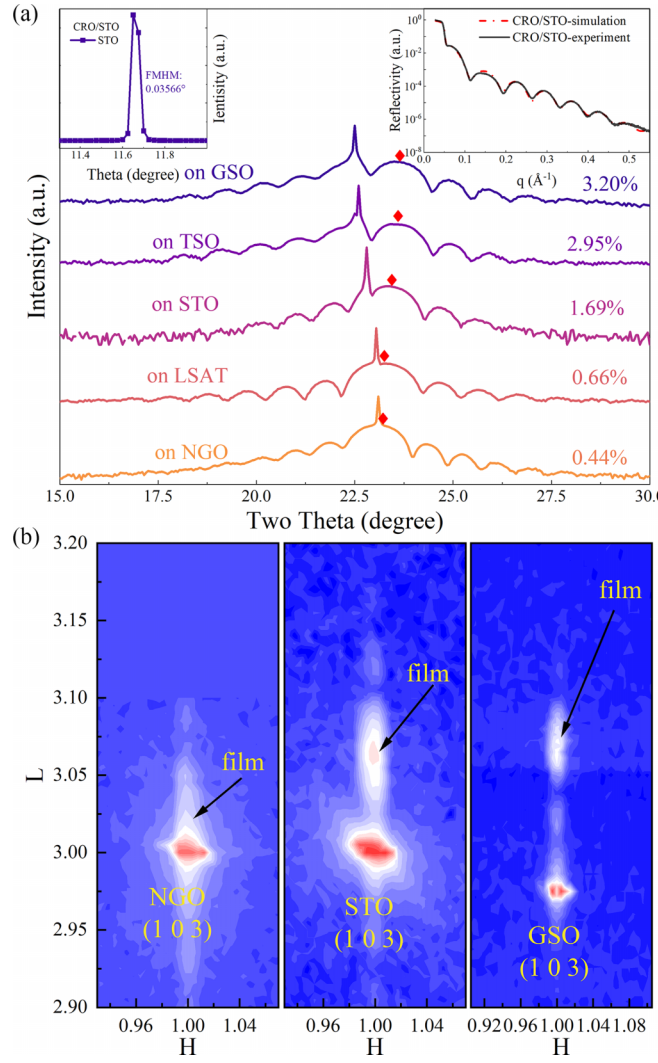

FIG. 1. (a) High-resolution θ-2θ scans ($\lambda = 1.5466$ Å) of $CaRuO_3$ thin films grown on NGO, LSAT, STO, TSO, and GSO substrates. The insets, from left to right, illustrate the rocking curve, experimental and fitted XRR curves of the $CaRuO_3$/STO thin film. (b) Representative RSMs around the (103) diffraction of $CaRuO_3$ films on NGO, STO, and GSO substrates. Note, all crystallographic indices are defined in the pseudocubic notation.

Results and Discussion. Figure 1(a) presents the (001) XRD patterns of our films, revealing shifts of peak positions as the substrate varies. The clear Laue oscillations around the (001) peak together with the sharp RC demonstrate smooth surfaces and commendable crystallinity. The film thickness was maintained at approximately 10 nm (∼26 u.c.), as evidenced from the XRR profile shown in the inset of Fig. 1(a). The RSMs of the $CaRuO_3$ films on different substrates [Fig. 1(b)] all indicate the complete coherence of the in-plane epitaxial strain.

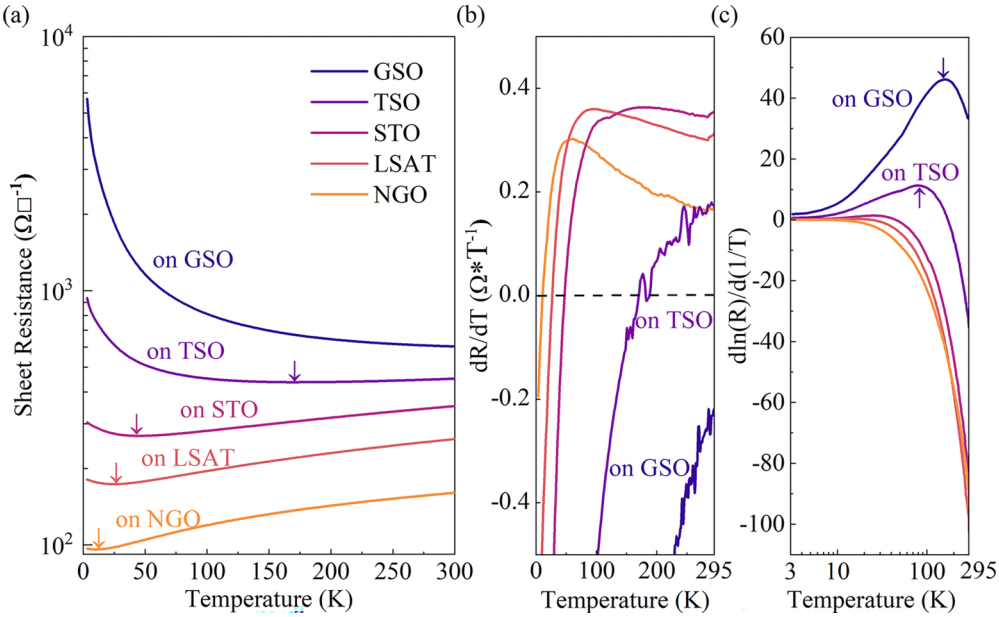

FIG. 2. (a) Temperature-dependent sheet resistances of $CaRuO_3$ thin films grown on NGO, LSAT, STO, TSO, and GSO substrates. The arrows indicate the characteristic temperature below which the resistivity upturn occurs. (b) dR/dT vs T plot for all samples to confirm the transition temperature. (c) Transport data of $CaRuO_3$ thin films have been analyzed in terms of $d(\ln(R))/d(1/T)$ vs T.

After confirming the structure quality of the $CaRuO_3$ films, we turn to explore their transport properties. As observed in Fig. 2(a), the temperature-dependent sheet resistance exhibits two distinct features. For films under smaller degrees of tensile strain (i.e., on NGO, LSAT, STO), an overall metallic behavior is observed with a low-temperature upturn as marked by arrows in the figure. Specifically, the onset of the upturn (denoted as T_{up}) is around 10 K on NGO substrate. T_{up} is enhanced with increasing the tensile strain, reaching ∼25 K on LSAT and ∼45 K on STO. However, the metallic behavior is nearly diminished on TSO substrate with T_{up} reaching ∼170 K, as reflected from the sign change of the slope on Fig. 2(b). Eventually, the $CaRuO_3$ film exhibits a complete semiconducting behavior on GSO substrate. In magnetic insulators or semiconductors, spin ordering typically leads to significant changes in the energy gap. Consequently, anomalies in the derivative $d(\ln(R))/d(1/T)$ are widely used to identify the magnetic transition temperature as it provides a temperature-dependent "gap" value. As shown in Fig. 2(c), under this analysis a distinct broad hump is observed for $CaRuO_3$ films on TSO and GSO substrates, with the maximum at ∼80 K and 160 K, respectively. This might indicate a plausible para to antiferromagnetic transition in these epitaxial $CaRuO_3$ films driven by the opening of a correlation gap, or the scales of the antiferromagnetic interactions triggered in these films [43,44].

In bulk $CaRuO_3$, the Ru 4d electrons establish the FL only at very low temperatures ($T_{FL} \sim 2$K), while the NFL behavior dominates at higher temperatures with the resistance exceeding the Mott-Ioffe-Regel (MIR) limit [45]. So we investigated the strain effect on the NFL behavior of the three samples that still fall within the metallic category ($CaRuO_3$ on NGO, LSAT, and STO). Fits of the power-law relationship $R - R_0 \propto T^n$ in the high-temperature range (100–300 K) were performed on these three samples [Fig. 3(a)]. The outcomes reveal that only the fit on $CaRuO_3$/NGO yields a similar behavior to the bulk, where the resistance is proportional to the square root of temperature. This is in reasonable accord with our expectation that NGO supplies the least tensile strain (∼0.44%). With increasing strain, for instance, on the LSAT substrate (∼0.66%), the power exponent n increases from 0.5 to 0.8, and further increases to 1 on STO (∼1.69%). These

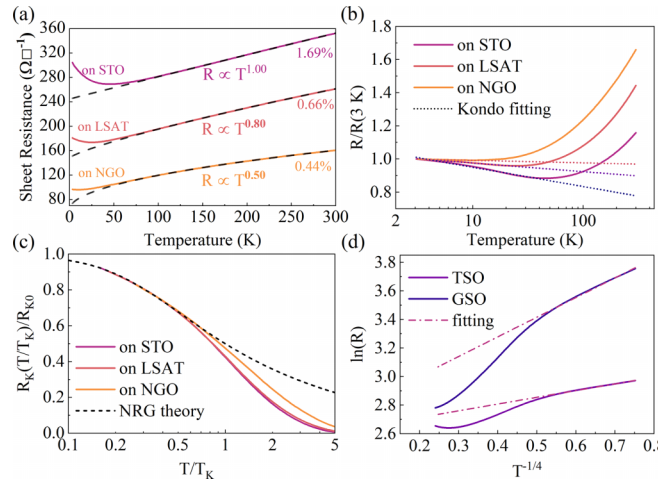

FIG. 3. For $CaRuO_3$ thin films on NGO, LSAT, and STO substrates, the fitting results of (a) power-law relationship for resistances at high-temperature regime; (b) Kondo effect for resistances at low-temperature regime. (c) Experimentally and theoretically [dashed line, numerical renormalization group (NRG)] scaled Kondo resistances $[R_K(T/T_K)/R_{K0}]$. For $CaRuO_3$ thin films on TSO and GSO substrates, the fitting results of (d) Mott type's VRH model $[\ln(R) \propto T^{-\frac{1}{4}}]$ at low-temperature regime.

results reveal that a moderate tensile strain can induce considerable variation on the collective behaviors of $CaRuO_3$ [14].

Based on the Hund's metal mechanism, in multiorbital compounds like $CaRuO_3$ and $SrRuO_3$ with non-half-filled d shells, the Hund's coupling drives the system away from the Mott transition and simultaneously enhances the electronic correlation by reducing the coherent size of quasiparticles [46–50]. That is why the values of T_{FL} are relatively small for both $CaRuO_3$ and $SrRuO_3$ [10,45]. Beyond this correlation scale, the system enters in an incoherent metallic state with "frozen" local magnetic moments, and shows the NFL behavior [49]. Notably, the notion of "frozen" local magnetic moments here differs from the random freezing of magnetic moments in a spin glass state. It refers to the persistence of local spin-spin correlation functions without decay over long periods, indicating the presence of strong local spin interactions in the system [49]. We tend to believe that variation of the NFL behavior in $CaRuO_3$ is related to the modulation of the strong local spin interactions.

Analyses on the low-temperature upturn behaviors of those three samples shed additional light on this interpretation. As depicted in Fig. 3(b) in terms of normalized resistance $R/R(3K)$, the upturn at low temperatures exhibits a tendency toward saturation, characteristic of the Kondo effect [51,52]. Indeed, despite employing various models such as a variable range hopping (VRH) model in different dimensions or a thermal activation model to attempt fitting, the upturn behavior of all three samples is best described by the Kondo effect. Specifically, the resistance can be expressed as

$$R(T) = R_0 + \alpha T^n + R_K(T/T_K),$$

where R_0 represents the residual resistance, the T^n term denotes the NFL behavior, and R_K is the resistance induced by the Kondo effect [53]. R_K is further expressed in a universal format with a single variable through the numerical renormalization group (NRG) theory [53–56]:

$$R_K\left(\frac{T}{T_K}\right) = R_{K0}[1 + (2^{1/s} - 1)(T/T_K)^2]^{-s}.$$

Here, T_K is the Kondo temperature; R_{K0} is the zero-temperature Kondo resistance; s determines the rate at which the resistance decreases with increasing temperature, with a value of 0.75 ± 0.02 for the three samples [53]. As shown in Fig. 3(c), following the Kondo scaling relationship, all the renormalized data fall onto one universal curve. The extracted values of the Kondo temperature T_K are ∼10 K for $CaRuO_3$ on NGO and ∼20 K on LSAT and STO. This is also consistent with the experimental trend observed in the high-temperature regime, corroborating the Kondo effect dominant over other origins such as electron-electron interaction [57,58] or weak localization [59–61].

Due to the strong local spin interactions, Ru 4d electrons exhibit dual characteristics of both itinerancy [11,12,62] and localization [63,64]. They serve as the charge carriers while also being responsible for providing the system with "frozen" local moments [49]. From this perspective, introduction of the Kondo effect in $CaRuO_3$ reflects the slowing down of the interconversion between the localized electrons with short-range magnetic interactions and the itinerant electrons among the Ru 4d orbitals. Macroscopically this manifests itself as "magnetic impurities," representing the enhanced electron localization and modulation of the overall NFL behavior in the high-temperature range.

In contrast, for the two samples exhibiting the semiconducting behavior ($CaRuO_3$ on TSO and GSO), we plot the curve of $R(T)$ against $1/T^\alpha$. As depicted in Fig. 3(d), the three-dimension VRH model, represented by $R(T) = R_0 e^{(\frac{T_0}{T})^{1/4}}$ with $\alpha = 1/4$, provides a reasonable description of the system's semiconducting behavior. This suggests that, unlike typical thermal excitations, the system exhibits strong localized states in the vicinity of the Fermi surface [65–67].

In Hund's metals, there is a crucial question regarding whether strong local spin interactions in the "spin-freezing" region can develop into long-range magnetic orders [10,45,49]. In the case of $SrRuO_3$, the itinerant ferromagnetism in the "spin-freezing" region has long been recognized. However, bulk $CaRuO_3$ does not develop any long-range magnetic order. This is likely attributed to the fact that the coherent length scale in $CaRuO_3$ is much shorter than that in $SrRuO_3$, and the electronic correlations in $CaRuO_3$, being stronger than in $SrRuO_3$, prevent short-range magnetic interactions within the "spin-freezing" region from evolving into long-range order [10,45]. Although this remains an open question, the presence of strong local spin interactions distinguishes it from trivial paramagnetic states. In this sense, whether it is the Kondo effect observed in the metallic phase of the three samples or the hump feature seen on $d(\ln R)/d(1/T)$ vs T plot for the semiconducting samples, both imply that the magnetic ground state may be modulated by epitaxial tensile strain.

Next we performed MR measurements on these $CaRuO_3$ thin films. Three representative behaviors are observed, as depicted in Fig. 4. For $CaRuO_3$ on NGO shown in Fig. 4(a), at temperatures $T \geqslant 20$ K, a positive MR is observed, with slightly increasing magnitude as temperature decreases. However, as the temperature further decreases, the positive MR is rapidly suppressed, and below 10 K, a negative MR is visible, and further temperature reduction amplifies its magnitude with the occurrence of a broad and weak hysteresis observed at $T = 2$ K. Note, unlike $CaRuO_3$ bulk which occurs at around 100 K [24], the temperature at which it switches to the negative MR effect has been greatly reduced in $CaRuO_3$ on NGO. Combined with the analyses of the low-temperature resistivity in Figs. 3(a) and 3(c), it can be inferred that the enhanced localization of Ru 4d electrons in the system manifests some characteristics resembling "magnetic impurities" on a macroscopic level. And it is the shielding effect of these so-called "magnetic impurities" that significantly reduces the temperature scale at which the system enters the negative MR. With strain increment, this shielding effect is gradually strengthened. As shown in Fig. 4(b) for $CaRuO_3$ on STO, although the strongest positive MR is seen around 20 K, the tendency toward the transition to negative MR is significantly suppressed down to the base temperature. It should be noted that the MR effects observed here are generally weak, with the magnitude less than 0.25%.

Figure 4(d) illustrates the variation of MR of four samples with temperatures under a 5 T magnetic field. Notably, the trends of the three metallic samples are basically in common, with slight changes in values. But the $CaRuO_3$/GSO sample

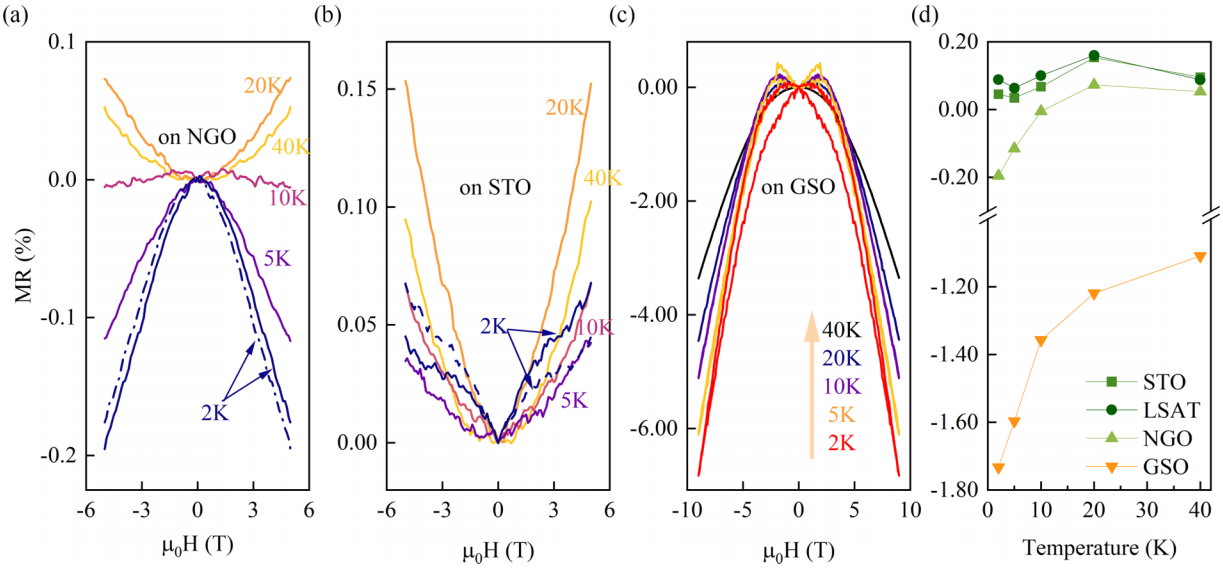

FIG. 4. Magnetoresistance of $CaRuO_3$ on (a) NGO, (b) STO, and (c) GSO with various temperatures as a function of magnetic field. (d) Magnetoresistance as a function of temperature at 5 T for $CaRuO_3$ films on NGO, LSAT, STO, and GSO substrates.

exhibits the distinct negative MR at low temperatures. Considering the strong correlation features of Hund's metal and the enhanced electron localization induced by strain, there are sufficient grounds to regard the semiconducting behavior as a Mott transition, yielding a Mott gap [45] associated with an antiferromagnetic ground state [68]. In this context, the transition observed in Fig. 2(c), as well as the negative MR and broad hysteresis displayed in Fig. 4(c), all reconcile with this scenario, with the magnetic ground state of $CaRuO_3$ from a paramagnetic state with strong local spin interactions to an antiferromagnetic state [69,70]. Nevertheless, more direct evidence is highly demanded through additional probes such as magnetic scattering experiments.

To better understand the experimental findings on strain-modulated magnetic and electronic configurations of $CaRuO_3$, we performed DFT + U calculations. Electronic and magnetic properties of (Ca, Sr)RuO_3 are significantly influenced by the on-site Coulomb correlations effects for Ru-4*d* electrons, as suggested by both experimental and theoretical studies [16,71,72]. To account for the on-site Coulomb interactions U among the Ru 4*d* electrons, we employed the rotationally invariant DFT + U method introduced by Liechtenstein *et al.* [73], with the parameter U set to 1 eV based on experimental findings [74]. DFT-optimized cell parameters of the unstrained structure are $a = 5.31$ Å, $b = 5.52$ Å, and $c = 7.62$ Å. The effect of in-plane biaxial strain was systematically investigated by varying the *a* and *b* lattice parameters in the range of -2% (compression) to $+8\%$ (tension) with a step size of $+1\%$, while freely relaxing the *c* lattice parameter. To determine the magnetic ground state under various biaxial strain conditions, we compared the total energy calculated for four distinct magnetic configurations with respect to that of the nonmagnetic (NM) configuration. The four considered magnetic configurations include one FM configuration and three distinct types of AFM configurations, namely, A, C, and G types [75]. Figure 5(a) shows the variation in the relative energies of distinct magnetic configurations calculated with respect to the total energy of the nonmagnetic configuration, as a function of biaxial strain. Our calculations reveal that when the biaxial strain $\leqslant 4\%$, the FM configuration possesses the lowest energy and stabilizes as the magnetic ground state. The result is consistent with what we observed in the experiment. $CaRuO_3$ is indeed not a simple paramagnet. Although it does not exhibit a long-range ferromagnetic order, a short-range ferromagnetic configuration might exist within the range of local spin interactions. It is noteworthy that in the FM phase, the oxygen atoms in $CaRuO_3$ contribute to the overall magnetization and may significantly influence the magnetic and electronic properties of $CaRuO_3$ near the Fermi level [74].

When the biaxial strain continues to increase, the calculated results indicate that the G-type AFM configuration becomes the lowest energy state, the critical value of strain (η_C) is about 4.5%. This aligns with our interpretation, corresponding to the transition of the magnetic ground state under high tensile strain. It is worth mentioning that the critical magnitude of the predicted biaxial strain in our DFT + U calculations is higher as compared to our experimental observations. This difference is mainly because, in our calculations, we are considering a bulk structure, thus straining infinite layers of the $CaRuO_3$ film. Furthermore, while the η_C at which the FM to AFM-G phase transition occurs is not highly sensitive to the value of U, we observed a systematic decrease in η_C with an increase in the U value [Fig. 5(b)].

In order to elucidate the electrical transport properties of the system, in the FM and G-type AFM configurations, the projected density of states (PDOS) computed along the high-symmetry directions using DFT + U in Ru 4*d* orbitals of $CaRuO_3$ while being subjected to biaxial strains is shown in Figs. 5(c)–5(h). The system shows a clear crystal field splitting of Ru 4*d* orbitals to t_{2g} and e_g states, due to the tilting and rotation of the RuO_6 octahedra. As can be seen from the distribution of PDOS, the e_g orbitals are nearly unoccupied while the t_{2g} orbitals are partially filled, suggesting the low spin configuration of Ru^{4+} ions, which demonstrates the validity of the calculations. From Figs. 5(c)–5(e), it can be observed

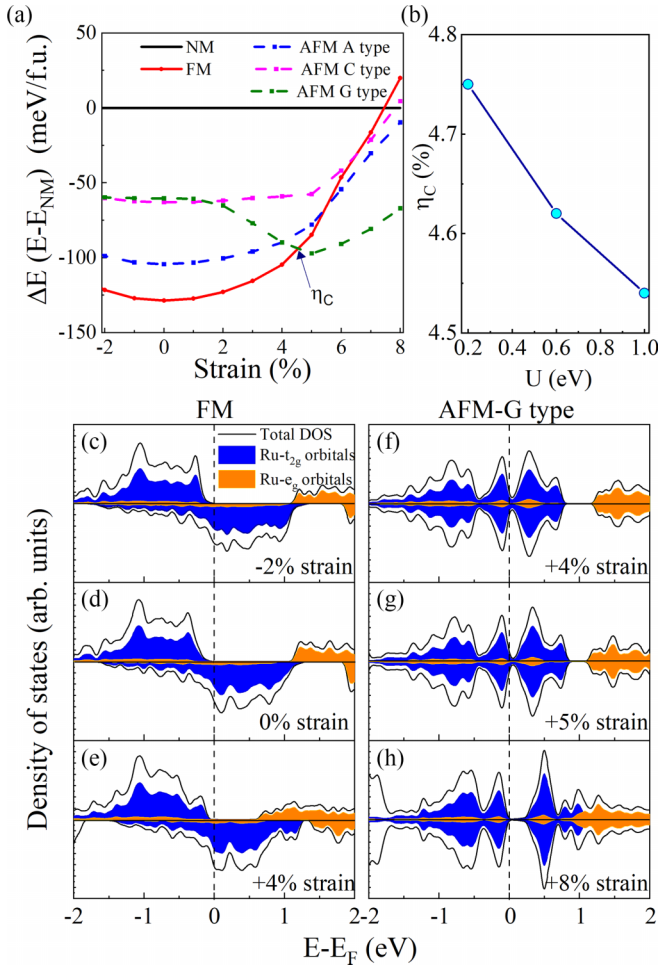

FIG. 5. (a) Variation of relative energies of nonmagnetic, FM, AFM-A, AFM-C, and AFM-G type configurations of $CaRuO_3$ with applied biaxial strains. (b) Variation of this critical strain η_C with U. (c)–(h) The atomic Ru *d* orbital projected DOS of strained $CaRuO_3$. Left panel: FM configuration under applied in-plane biaxial strains of (c) x = −2%, (d) x = 0%, and (e) x = +4%; Right panel: AFM-G type configuration under applied in-plane biaxial strains of (f) x = +4%, (g) x = +5%, and (h) x = +8%. The black line shows the total density of states, the blue color represents the projected DOS of t_{2g} orbitals of Ru, while the orange color represents the projection of e_g orbitals. The vertical, black dotted line represents the Fermi level.

that when strain is within 4%, the FM configuration exhibits relatively large PDOS on the Fermi surface, indicating overall metallic behaviors of the system. However, for strain $\geqslant$ 4%, adopting the G-type AFM configuration, the PDOS on the Fermi surface becomes finite with a gap opening, as shown in Figs. 5(f)–5(h). This implies that the system undergoes a MIT under high strain status, accompanied by a transition in the magnetic ground state. This is consistent with our experimental observations.

Conclusion. We synthesized (001)-oriented 10 nm $CaRuO_3$ thin films on different substrates and investigated their electronic and magnetic properties through various transport measurements and DFT + U calculations. The experimental results indicate that even a small amount of tensile strain can introduce the Kondo effect in $CaRuO_3$, thin films, leading to significant modulation of the NFL behavior and MR. Especially, when the strain reaches a certain threshold, the $CaRuO_3$ undergoes a metal-semiconductor transition, likely accompanied by a phase transition in the magnetic ground state. Combining our experiments with theoretical calculations, we suggest that the magnetic state possesses a G-type antiferromagnetic order. These findings are crucial for understanding the strongly correlated metallic nature of $CaRuO_3$, and the emergence of an antiferromagnetic state under large tensile strain represents an intriguing hidden aspect, highlighting the potential of $CaRuO_3$ thin films as promising platforms for investigating quantum phase transition and critical behaviors.

Acknowledgments. This research is supported by the International Partnership Program of Chinese Academy of Sciences under Grant No. 113111KYSB20190052 and by National Natural Science Foundation of China under Contract No. U1532104. This work is supported by the National Key R&D Program of China (Grant No. 2022YFA1403000), the National Natural Science Foundation of China (Grants No. 12204521 and No. 12250710675), and the Strategic Priority Research Program of the Chinese Academy of Sciences (No. XDB33000000). A portion of this work was carried out at the Synergetic Extreme Condition User Facility (SECUF). A portion of this work was based on the data obtained at beamline 1W1A of the Beijing Synchrotron Radiation Facility (BSRF-1W1A). A.B. and S.S. acknowledge support from the University Research Awards at the University of Rochester.

[1] J. Ngai, F. Walker, and C. Ahn, Correlated oxide physics and electronics, Annu. Rev. Mater. Res. **44**, 1 (2014).
[2] H. Takagi and H. Y. Hwang, An emergent change of phase for electronics, Science **327**, 1601 (2010).
[3] M. Imada, A. Fujimori, and Y. Tokura, Metal-insulator transitions, Rev. Mod. Phys. **70**, 1039 (1998).
[4] W. E. Pickett, Electronic structure of the high-temperature oxide superconductors, Rev. Mod. Phys. **61**, 433 (1989).
[5] E. Dagotto, Complexity in strongly correlated electronic systems, Science **309**, 257 (2005).
[6] H.-A. Krug Von Nidda, R. Bulla, N. Büttgen, M. Heinrich, and A. Loidl, Heavy fermions in transition metals and transition-metal oxides, Eur. Phys. J. B **34**, 399 (2003).
[7] E. Morosan, D. Natelson, A. H. Nevidomskyy, and Q. Si, Strongly correlated materials, Adv. Mater. **24**, 4896 (2012).
[8] C.-W. Chen, J. Choe, and E. Morosan, Charge density waves in strongly correlated electron systems, Rep. Prog. Phys. **79**, 084505 (2016).
[9] C. M. Varma, Z. Nussinov, and W. van Saarloos, Singular or non-Fermi liquids, Phys. Rep. **361**, 267 (2002).
[10] G. R. Stewart, Non-Fermi-liquid behavior in *d*- and *f*-electron metals, Rev. Mod. Phys. **73**, 797 (2001).
[11] G. Koster, L. Klein, W. Siemons, G. Rijnders, J. S. Dodge, C.-B. Eom, D. H. A. Blank, and M. R. Beasley, Structure, physical properties, and applications of $SrRuO_3$ thin films, Rev. Mod. Phys. **84**, 253 (2012).

[12] Y. Gu, Q. Wang, W. Hu, W. Liu, Z. Zhang, F. Pan, and C. Song, An overview of $SrRuO_3$-based heterostructures for spintronic and topological phenomena, J. Phys. D: Appl. Phys. **55**, 233001 (2022).

[13] J. M. Longo, P. M. Raccah, and J. B. Goodenough, Magnetic properties of $SrRuO_3$ and $CaRuO_3$, J. Appl. Phys. **39**, 1327 (1968).

[14] H. T. Dang, J. Mravlje, A. Georges, and A. J. Millis, Electronic correlations, magnetism, and Hund's rule coupling in the ruthenium perovskites $SrRuO_3$ and $CaRuO_3$, Phys. Rev. B **91**, 195149 (2015).

[15] E. Jakobi, S. Kanungo, S. Sarkar, S. Schmitt, and T. Saha-Dasgupta, LDA + DMFT study of Ru-based perovskite $SrRuO_3$ and $CaRuO_3$, Phys. Rev. B **83**, 041103 (2011).

[16] A. T. Zayak, X. Huang, J. B. Neaton, and K. M. Rabe, Structural, electronic, and magnetic properties of $SrRuO_3$ under epitaxial strain, Phys. Rev. B **74**, 094104 (2006).

[17] S. Shen, Z. Li, Z. Tian, W. Luo, S. Okamoto, and P. Yu, Emergent ferromagnetism with fermi-liquid behavior in proton intercalated $CaRuO_3$, Phys. Rev. X **11**, 021018 (2021).

[18] P. Kostic, Y. Okada, N. C. Collins, Z. Schlesinger, J. W. Reiner, L. Klein, A. Kapitulnik, T. H. Geballe, and M. R. Beasley, Non-Fermi-liquid behavior of $SrRuO_3$: Evidence from infrared conductivity, Phys. Rev. Lett. **81**, 2498 (1998).

[19] Z. Ding, X. Chen, Z. Wang, Q. Zhang, F. Yang, J. Bi, T. Lin, Z. Wang, X. Wu, M. Gu, M. Meng, Y. Cao, L. Gu, J. Zhang, Z. Zhong, X. Liu, and J. Guo, Magnetism and berry phase manipulation in an emergent structure of perovskite ruthenate by (111) strain engineering, npj Quantum Mater. **8**, 43 (2023).

[20] L. M. Wang, H. E. Horng, and H. C. Yang, Anomalous magnetotransport in $SrRuO_3$ films: A crossover from Fermi-liquid to non-Fermi-liquid behavior, Phys. Rev. B **70**, 014433 (2004).

[21] O. Morán, W. Saldarriaga, and E. Baca, Possible occurrence of transition from a Fermi- to a non-Fermi-liquid behavior in epitaxial $SrRuO_3$ thin films, Superlattices Microstruct. **55**, 151 (2013).

[22] W. Shi, J. Zhang, X. Chen, Q. Zhang, X. Zhan, Z. Li, J. Zheng, M. Wang, F. Han, H. Zhang, L. Gu, T. Zhu, B. Liu, Y. Chen, F. Hu, B. Shen, Y. Chen, and J. Sun, Symmetry-mismatch-induced ferromagnetism in the interfacial layers of $CaRuO_3/SrTiO_3$ superlattices, Adv. Funct. Mater. **33**, 2300338 (2023).

[23] M. Schneider, D. Geiger, S. Esser, U. S. Pracht, C. Stingl, Y. Tokiwa, V. Moshnyaga, I. Sheikin, J. Mravlje, M. Scheffler, and P. Gegenwart, Low-energy electronic properties of clean $CaRuO_3$: Elusive landau quasiparticles, Phys. Rev. Lett. **112**, 206403 (2014).

[24] L. Klein, L. Antognazza, T. H. Geballe, M. R. Beasley, and A. Kapitulnik, Possible non-Fermi-liquid behavior of $CaRuO_3$, Phys. Rev. B **60**, 1448 (1999).

[25] M. S. Laad and E. Müller-Hartmann, Origin of the non-Fermi liquid behavior of $SrRuO_3$, Phys. Rev. Lett. **87**, 246402 (2001).

[26] I. Felner, I. Nowik, I. Bradaric, and M. Gospodinov, $CaRuO_3$ is not a paramagnetic material, Phys. Rev. B **62**, 11332 (2000).

[27] K. Yoshimura, T. Imai, T. Kiyama, K. R. Thurber, A. W. Hunt, and K. Kosuge, ^{17}O NMR observation of universal behavior of ferromagnetic spin fluctuations in the itinerant magnetic system $Sr_{1-x}Ca_xRuO_3$, Phys. Rev. Lett. **83**, 4397 (1999).

[28] M. Yokoyama, S. Nakano, S. Someya, T. Nakada, N. Wada, H. Kawanaka, H. Bando, K. Tenya, A. Kondo, and K. Kindo, Low-temperature specific heat for ferromagnetic and antiferromagnetic orders in $CaRu_{1-x}Mn_xO_3$, J. Phys.: Conf. Ser. **391**, 012114 (2012).

[29] N. Hosaka, H. Yamada, Y. Shimada, J. Fujioka, S. Bordács, I. Kézsmárki, M. Kawasaki, and Y. Tokura, Magneto-optical characterization on the ferromagnetic-paramagnetic transitions in the composition-spread epitaxial film of $Sr_{1-x}Ca_xRuO_3$, Appl. Phys. Express **1**, 113001 (2008).

[30] P. Ravindran, R. Vidya, P. Vajeeston, A. Kjekshus, H. Fjellvåg, and B. Hauback, Antiferromagnetic vs. ferromagnetic interactions and spin-glass-like behavior in ruthenates, Solid State Commun. **124**, 293 (2002).

[31] Z. Ali, M. Saghayezhian, Z. Wang, A. O'Hara, D. Shin, W. Ge, Y. T. Chan, Y. Zhu, W. Wu, S. T. Pantelides, and J. Zhang, Emergent ferromagnetism and insulator-metal transition in δ-doped ultrathin ruthenates, npj Quantum Mater. **7**, 108 (2022).

[32] A. T. Zayak, X. Huang, J. B. Neaton, and K. M. Rabe, Manipulating magnetic properties of $SrRuO_3$ and $CaRuO_3$ with epitaxial and uniaxial strains, Phys. Rev. B **77**, 214410 (2008).

[33] S. Middey, P. Mahadevan, and D. D. Sarma, Dependence of magnetism on $GdFeO_3$ distortion in the t_{2g} system $ARuO_3$ (A = Sr,Ca), Phys. Rev. B **83**, 014416 (2011).

[34] P. Hohenberg and W. Kohn, Inhomogeneous electron gas, Phys. Rev. **136**, B864 (1964).

[35] W. Kohn and L. J. Sham, Self-consistent equations including exchange and correlation effects, Phys. Rev. **140**, A1133 (1965).

[36] P. E. Blöchl, Projector augmented-wave method, Phys. Rev. B **50**, 17953 (1994).

[37] G. Kresse and J. Furthmüller, Efficient iterative schemes for *ab initio* total-energy calculations using a plane-wave basis set, Phys. Rev. B **54**, 11169 (1996).

[38] G. Kresse and J. Furthmüller, Efficiency of *ab-initio* total energy calculations for metals and semiconductors using a plane-wave basis set, Comput. Mater. Sci. **6**, 15 (1996).

[39] G. Kresse and D. Joubert, From ultrasoft pseudopotentials to the projector augmented-wave method, Phys. Rev. B **59**, 1758 (1999).

[40] H. J. Monkhorst and J. D. Pack, Special points for brillouin-zone integrations, Phys. Rev. B **13**, 5188 (1976).

[41] J. P. Perdew, A. Ruzsinszky, G. I. Csonka, O. A. Vydrov, G. E. Scuseria, L. A. Constantin, X. Zhou, and K. Burke, Restoring the density-gradient expansion for exchange in solids and surfaces, Phys. Rev. Lett. **100**, 136406 (2008).

[42] V. Wang, N. Xu, J.-C. Liu, G. Tang, and W.-T. Geng, VASPKIT: A user-friendly interface facilitating high-throughput computing and analysis using VASP code, Comput. Phys. Commun. **267**, 108033 (2021).

[43] J.-S. Zhou, J. B. Goodenough, and B. Dabrowski, Exchange interaction in the insulating phase of $RNiO_3$, Phys. Rev. Lett. **95**, 127204 (2005).

[44] S. K. Ojha, S. Ray, T. Das, S. Middey, S. Sarkar, P. Mahadevan, Z. Wang, Y. Zhu, X. Liu, M. Kareev, and J. Chakhalian, Anomalous electron transport in epitaxial $NdNiO_3$ films, Phys. Rev. B **99**, 235153 (2019).

[45] A. Georges, L. D. Medici, and J. Mravlje, Strong correlations from Hunds coupling, Annu. Rev. Condens. Matter Phys. **4**, 137 (2013).

[46] Z. P. Yin, K. Haule, and G. Kotliar, Kinetic frustration and the nature of the magnetic and paramagnetic states in iron pnictides and iron chalcogenides, Nat. Mater. **10**, 932 (2011).

[47] D. van der Marel and G. A. Sawatzky, Electron-electron interaction and localization in *d* and *f* transition metals, Phys. Rev. B **37**, 10674 (1988).

[48] I. Okada and K. Yosida, Singlet ground state of the localized *d*-electrons coupled with conduction electrons in metals, Prog. Theor. Phys. **49**, 1483 (1973).

[49] P. Werner, E. Gull, M. Troyer, and A. J. Millis, Spin freezing transition and non-fermi-liquid self-energy in a three-orbital model, Phys. Rev. Lett. **101**, 166405 (2008).

[50] J. Mravlje, M. Aichhorn, T. Miyake, K. Haule, G. Kotliar, and A. Georges, Coherence-incoherence crossover and the mass-renormalization puzzles in Sr_2RuO_4, Phys. Rev. Lett. **106**, 096401 (2011).

[51] G. M. De Luca, R. Di Capua, E. Di Gennaro, F. M. Granozio, D. Stornaiuolo, M. Salluzzo, A. Gadaleta, I. Pallecchi, D. Marrè, C. Piamonteze, M. Radovic, Z. Ristic, and S. Rusponi, Transport properties of a quasi-two-dimensional electron system formed in $LaAlO_3/EuTiO_3/SrTiO_3$ heterostructures, Phys. Rev. B **89**, 224413 (2014).

[52] S. Das, P. C. Joshi, A. Rastogi, Z. Hossain, and R. C. Budhani, Magnetothermopower of δ-doped $LaTiO_3/SrTiO_3$ interfaces in the Kondo regime, Phys. Rev. B **90**, 075133 (2014).

[53] D. Goldhaber-Gordon, J. Göres, M. A. Kastner, H. Shtrikman, D. Mahalu, and U. Meirav, From the Kondo regime to the mixed-valence regime in a single-electron transistor, Phys. Rev. Lett. **81**, 5225 (1998).

[54] F. Yang, Z. Wang, Y. Liu, S. Yang, Z. Yu, Q. An, Z. Ding, F. Meng, Y. Cao, Q. Zhang, L. Gu, M. Liu, Y. Li, J. Guo, and X. Liu, Engineered Kondo screening and nonzero Berry phase in $SrTiO_3/LaTiO_3/SrTiO_3$ heterostructures, Phys. Rev. B **106**, 165421 (2022).

[55] Y. Cao, Z. Yang, M. Kareev, X. Liu, D. Meyers, S. Middey, D. Choudhury, P. Shafer, J. Guo, J. W. Freeland, E. Arenholz, L. Gu, and J. Chakhalian, Magnetic interactions at the nanoscale in trilayer titanates, Phys. Rev. Lett. **116**, 076802 (2016).

[56] T. Sugiyama and N. Tsuda, Kondo effect in the resistivity of $CaRu_{1-x}Mn_xO_3$, J. Phys. Soc. Jpn. **68**, 1306 (1999).

[57] H. Wang, H. Liu, C.-Z. Chang, H. Zuo, Y. Zhao, Y. Sun, Z. Xia, K. He, X. Ma, X. C. Xie, Q.-K. Xue, and J. Wang, Crossover between weak antilocalization and weak localization of bulk states in ultrathin Bi_2Se_3 films, Sci. Rep. **4**, 5817 (2014).

[58] J. Wang, A. M. DaSilva, C.-Z. Chang, K. He, J. K. Jain, N. Samarth, X.-C. Ma, Q.-K. Xue, and M. H. W. Chan, Evidence for electron-electron interaction in topological insulator thin films, Phys. Rev. B **83**, 245438 (2011).

[59] G. Bergmann, Weak localization in thin films: a time-of-flight experiment with conduction electrons, Phys. Rep. **107**, 1 (1984).

[60] M. Y. Simmons, A. R. Hamilton, M. Pepper, E. H. Linfield, P. D. Rose, and D. A. Ritchie, Weak localization, hole-hole interactions, and the metal-insulator transition in two dimensions, Phys. Rev. Lett. **84**, 2489 (2000).

[61] G. Bergmann, Weak anti-localization An experimental proof for the destructive interference of rotated spin, Solid State Commun. **42**, 815 (1982).

[62] D. J. Singh, Electronic and magnetic properties of the 4*d* itinerant ferromagnet $SrRuO_3$, J. Appl. Phys. **79**, 4818 (1996).

[63] D. Toyota, I. Ohkubo, H. Kumigashira, M. Oshima, T. Ohnishi, M. Lippmaa, M. Takizawa, A. Fujimori, K. Ono, M. Kawasaki, and H. Koinuma, Thickness-dependent electronic structure of ultrathin $SrRuO_3$ films studied by *in situ* photoemission spectroscopy, Appl. Phys. Lett. **87**, 162508 (2005).

[64] M. Takizawa, D. Toyota, H. Wadati, A. Chikamatsu, H. Kumigashira, A. Fujimori, M. Oshima, Z. Fang, M. Lippmaa, M. Kawasaki, and H. Koinuma, Manifestation of correlation effects in the photoemission spectra of $Ca_{1-x}Sr_xRuO_3$, Phys. Rev. B **72**, 060404(R) (2005).

[65] J. J. Ishikawa, E. C. T. O'Farrell, and S. Nakatsuji, Continuous transition between antiferromagnetic insulator and paramagnetic metal in the pyrochlore iridate $Eu_2Ir_2O_7$, Phys. Rev. B **85**, 245109 (2012).

[66] J. Hemberger, H.-A. K. Von Nidda, V. Fritsch, J. Deisenhofer, S. Lobina, T. Rudolf, P. Lunkenheimer, F. Lichtenberg, A. Loidl, D. Bruns, and B. Büchner, Evidence for Jahn-Teller distortions at the antiferromagnetic transition in $LaTiO_3$, Phys. Rev. Lett. **91**, 066403 (2003).

[67] S. Lamba and D. Kumar, Variable-range hopping: Role of Coulomb interactions, Phys. Rev. B **59**, 4752 (1999).

[68] A. V. Puchkov, M. C. Schabel, D. N. Basov, T. Startseva, G. Cao, T. Timusk, and Z.-X. Shen, Layered ruthenium oxides: From band metal to Mott insulator, Phys. Rev. Lett. **81**, 2747 (1998).

[69] H. Wang, C. Lu, J. Chen, Y. Liu, S. L. Yuan, S.-W. Cheong, S. Dong, and J.-M. Liu, Giant anisotropic magnetoresistance and nonvolatile memory in canted antiferromagnet Sr_2IrO_4, Nat. Commun. **10**, 2280 (2019).

[70] J. Matsuno, K. Ihara, S. Yamamura, H. Wadati, K. Ishii, V. V. Shankar, H.-Y. Kee, and H. Takagi, Engineering a spin-orbital magnetic insulator by tailoring superlattices, Phys. Rev. Lett. **114**, 247209 (2015).

[71] J. S. Ahn, J. Bak, H. S. Choi, T. W. Noh, J. E. Han, Y. Bang, J. H. Cho, and Q. X. Jia, Spectral evolution in $(Ca, Sr)RuO_3$ near the Mott-Hubbard transition, Phys. Rev. Lett. **82**, 5321 (1999).

[72] J. M. Rondinelli, N. M. Caffrey, S. Sanvito, and N. A. Spaldin, Electronic properties of bulk and thin film $SrRuO_3$: Search for the metal-insulator transition, Phys. Rev. B **78**, 155107 (2008).

[73] A. I. Liechtenstein, V. I. Anisimov, and J. Zaanen, Density-functional theory and strong interactions: Orbital ordering in Mott-Hubbard insulators, Phys. Rev. B **52**, R5467 (1995).

[74] See Supplemental Material at http://link.aps.org/supplemental/10.1103/PhysRevB.110.L041403 for more details about film quality characterizations, DFT calculation results with different U values, and discussions about the local magnetic moments of the explored phases.

[75] Due to the limitations of aptly simulating the paramagnetic phase within the DFT+U approach, we decided to use the energies calculated for the nonmagnetic configuration as the reference to determine the relative stability of different magnetic phases.